Effect of Alloying Elements on Microstructure and Mechanical Properties of Air-Cooled Bainitic Steel

MINAL SHAH, S.K. DAS, and S. GHOSH CHOWDHURY

In the present investigation, a carbide-free bainitic steel has been produced in the laboratory through the air cooling route. Optimization of the alloying elements was done based on thermodynamic and kinetic calculations. Emphasis was given to obtain ultrafine bainitic microstructure by maximizing the driving force and lowering the transformation temperature of bainite formation. In addition to bainite, the microstructure contained a small amount of austenite and martensite. It was observed that Mn decreases $\Delta G^{\gamma \rightarrow \alpha}$ to a greater extent as compared to Cr and Si. Therefore, a low Mn-high Cr alloy exhibited large driving force and low B_s temperature. Si promoted carbon partitioning in the adjacent austenite to make it more stable. Therefore, the transformation of deformation-induced martensite from the retained austenite during the deformation process was restricted, resulting in higher toughness of the alloy. Thus, the air-cooled bainitic steel produced in lab scale showed better strength, toughness, and hardness than the conventional bainitic steel produced by the isothermal route.

https://doi.org/10.1007/s11661-019-05177-1

I. INTRODUCTION

BAINITIC steel with fine bainitic laths and film type of retained austenite sandwiched between two bainitic laths are proven to provide a good combination of strength and toughness.[1,2] Such steels are developed by two-stage processing with heat treating the steel to the austenite zone and cooling subsequently to a bainitic bay. Further, the steel is isothermally heat treated in a bainitic bay for a period until the formation of bainite and is subsequently cooled to room temperature.[3,4]

However, instead of the two-stage cost of intense processing to obtain a desired combination of strength toughness, an air-cooled bainitic steel could provide a cost-effective material with the desired properties.[3,4] In this respect, attempts have been made either by alloy modification or altering the processing route. The generic design principles of such steels were explored by Gomez *et al.*,[3,4] and they used Mn content of < 0.1 wt pct to avoid banding in bainitic steel during solidification.[3] Nickel is also added in such steel to improve the toughness of steel by stabilizing the retained austenite. Lowering of Cr content was done to maximize the amount of bainitic transformation, and Al was added in a small amount for deoxidation.[3] Sourmail *et al.*[5] reported the possibility of carbide-free bainite formation during air cooling. In terms of process modification, isothermal treatment was considered for obtaining ultrafine high strength steel.[6,7] However, the process is not economically viable because of the long holding time required for isothermal treatment. Adjustment of composition in the steel is one of the preferred routes to obtain bainitic microstructure during air cooling after austenitization.[5,6,8] It is reported that the air-cooled bainitic steel has a higher amount of bainite and better mechanical properties than austempered bainitic steel.[9] Continuously cooled bainitic steel has shown a very good combination of strength and toughness.[5,6] Das and Haldar[8] made an attempt to design bainitic steel that could be produced directly in a hot strip mill by accelerated cooling on the run-out table followed by coiling and reported a tensile strength of ~ 1370 MPa with ductility of 21 pct.[8] Phases, such as allotriomorphic ferrite, Widmanstätten ferrite, martensite, and blocky austenite, are to be avoided to improve the toughness of the steel.[10] Other researchers[11–15] reported that carbide-free bainite microstructure with high silicon provides very good wear resistance (rolling/sliding). The unique combination of strength and toughness of high Si bainitic steel were attributed to the synergistic effect of ultrafine microstructure and absence of coarse carbides.[11–15] Fang *et al.*[16] reported the development of manganese containing carbide-free

MINAL SHAH, S.K. DAS, and S. GHOSH CHOWDHURY are with the Materials Engineering Division, CSIR-National Metallurgical Laboratory, Jamshedpur, 831007, India. Contact e-mail: minalshah@nmlindia.org
Manuscript submitted August 21, 2017.
Article published online March 12, 2019

bainite/martensite steel by air cooling; however, this steel contained granular bainite, which was undesirable considering the poor toughness of steel. A continuous cooling transformation (CCT) diagram for low-carbon microalloyed steels under the simulated welding thermal cycle process (10 to 600 seconds) was developed by Kong and Qiu.[17] They showed that the faster cooling rate resulted in the formation of a mixture of bainite and martensite, whereas the slower cooling rate resulted in the formation of granular bainite. It was also reported that the granular bainite formed due to a slower cooling rate possessed lesser toughness than the acicular ferrite formed in the weld metal.[18] The effect of Mn on the bainitic transformation in the weld metal was studied by Keehan *et al.*[19] Formation of coalesced bainite resulted in a lower impact toughness in the weld metal with 2 wt pct Mn in comparison to 0.5 wt pct Mn. Mo addition was done to eliminate austenite grain boundary embrittlement caused by phosphorus. Fine bainite formation was reported in 0.30 to 0.35 wt pct C steel.[8] In all the preceding illustrations, the main disadvantage is the use of a higher extent of carbon (0.25 to 0.35 wt pct) in the alloys. Carbon in this range generally deteriorates the weldability of the steel. Also, in a few cases, Ni and other costly alloying elements were used. To eradicate the preceding limitation, in the present endeavor, a new generation of air-cooled bainitic steel with improved properties was developed in a laboratory scale. A major thrust has been given on (1) the reduction in carbon content along with readjustment of the composition of steel and (2) the co-relation between the mechanical behaviors of the alloy with the processing route for optimizing the alloy design parameters.

II. ALLOY DESIGN

A. *Strengthening Mechanism of the Steel*

For steels having predominantly bainite and austenite microstructures, the sources of strengthening are limited. The contribution toward strength comes from solid solution strengthening of phases, dislocations that are generated during bainitic transformation, and the presence of fine bainitic laths. The theoretical strength of such microstructures can be expressed as[20]

$$\sigma = \sigma_{\mathrm{Fe}} + \sum \sigma_{\mathrm{ss},i} + \sigma_C + K_L \overline{L}^{-1} + K_D \rho_D^{\frac{1}{2}} + K_P \delta^{-1} \quad [1]$$

where K_L, K_D, and K_P are constants, σ_{Fe} is the strength of pure annealed iron, $\sigma_{ss,\mathrm{i}}$ is the solid solution strengthening due to substitutional elements i, σ_C is the solid solution strengthening due to carbon, $\overline{L}$ is the bainitic ferrite plate thickness, ρ_D is the dislocation density, and is the distance between successive carbide particles. For carbide-free bainitic steels, the last term can be ignored. The effect of solid solution strengthening can be illustrated per Table I, which shows the contributions for different alloying elements.[21] The dislocation density of bainite can be empirically given by Reference 20. For the calculation of the dislocation density, an average of bainitic start and martensite start temperatures is considered to be the transformation temperature for bainite formation:

Table I. Solid Solution Strengthening Components in Low-Temperature Bainite[21]

Elements	Strength Contributions
C	(wt pct C)$^{1/2}$ × 1722.5
Si	wt pct Si × 85 MPa/wt pct
Mn	wt pct Mn × 32 MPa/wt pct
Mo	wt pct Mo × 30 MPa/wt pct
Cr	wt pct Cr × − 30 MPa/wt pct
V	wt pct V × 9 MPa/wt pct

$$\log(\rho_D) = 9.2820 + \frac{6880.73}{T} - \frac{1,780,360}{T^2} \quad [2]$$

where ρ_D is the dislocation density (length/m^3) and T is the absolute temperature in degree Kelvin. The strengthening due to dislocation can be estimated as[22]

$$\sigma_\rho = 0.38 \mu \mathrm{b} \rho_D^{1/2} \quad [3]$$

where μ and b are the shear modulus and the magnitude of the Burgers vector, respectively. Low transformation temperature is desirable for high dislocation density. In bainitic steels, the strengthening term σ_G is due to the fine lath structure of bainite, which depends inversely on the mean value of the larger diameter of slip planes. The mean slip plane diameter is governed by the thickness of the plates/lath and may be correlated in the form of Eq. [4].[23] A transmission electron microscope (TEM) is used to determine the true plate thickness of bainite, t, by measuring the mean linear intercept $\overline{L}$ in a direction normal to the bainite plate length:

$$\overline{L} = \frac{\pi t}{2} \quad [4]$$

where $\overline{L}$ is the mean lineal intercept measured at random operations on random sections. The strengthening, which can then be expected from fine plates or laths of bainite, can be estimated as[20,24,25]

$$\sigma_G = \frac{115}{\overline{L}} \quad [5]$$

Thus, the bainite lath thickness is an important parameter. The thickness of the bainite lath in a silicon-rich steel depends primarily on the characteristics of the austenite phase at the transformation temperature, the austenite strength, and the chemical-free energy available for the bainite transformation.[26] Using the preceding empirical relations and reconsidering the aim of the investigation, the following aspects were considered during design of the alloys.

(1) Air cooling is faster than the isothermal or austempering process. Si and Al restrict the formation of cementite owing to the slower kinetics of cementite precipitation in air-cooled bainite.[27–29]

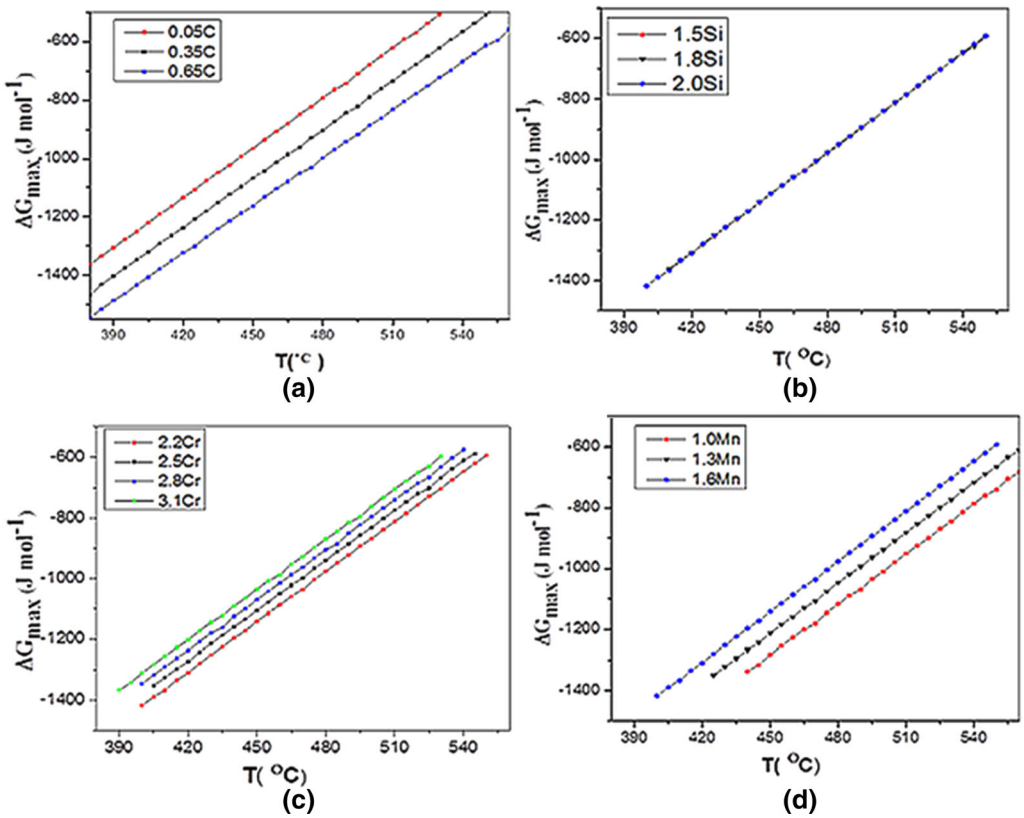

Fig. 1—Effect of alloying elements in the free energy of transformation of bainite: (*a*) carbon, (*b*) silicon, (*c*) chromium, and (*d*) manganese.

(2) Total alloy content should be such that the fine bainitic lath can be produced when B_s becomes < 500 °C and the bainite nose temperature is sufficiently above the martensite start temperature.
(3) With the given composition, complete single-phase solid solution can be achieved at 1000 °C to 1250 °C and under normal air cooling (0.1 °C/s to 0.5 °C/s) bainite can be produced.[4]
(4) It is desirable that the final microstructure of the steel would consist of carbide-free bainite, films of retained austenite, and a minimum amount of martensite.
(5) The presence of blocky austenite is not desirable in the final microstructure as it transforms into martensite.[27] The formation of martensite can be restricted by ensuring adequate carbon concentration in austenite. The carbon content can be altered by shifting the T_0 temperature to a higher carbon concentration, c_{T0}; the bainitic transformation temperature (T) can be reduced to increase c_{T0}; the average carbon concentration, $\overline{c}$, of the steel can also be reduced to increase the volume fraction of bainite and, hence, austenite blocks can be consumed:[7,30]

$$V_b = \frac{C_{T0} - \overline{C}}{(C_{T0} - C_{\alpha b})} \quad [6]$$

where V_b is the maximum volume fraction of bainite that can form and $c_{\alpha b}$ is the carbon content that remains in the bainite after the excess has been partitioned into the retained austenite.
(6) Avoidance of allotriomorphic ferrite, Widmanstätten ferrite, and pearlite formation is necessary to reduce heterogeneity in the structure.[4]

B. *Thermodynamic Evaluation*

To promote bainitic transformation, a few thermodynamic conditions are illustrated in the open domain literature.[30] $\Delta G^{\gamma \to \alpha}$ should be as negative as possible so that a greater volume fraction of the refined microstructure can be obtained. The effect of alloying elements has been studied through a Fortran computer program, combined with Thermo-Calc to calculate the Gibbs free energy of bainite formation (Figure 1).[31]

It can be seen from Figure 1(a) that carbon plays a dominant role in the reduction of $\Delta G^{\gamma \to \alpha}$. The increment of carbon to the tune of ~ 0.3 wt pct reduces $|\Delta G^{\gamma \to \alpha}|$ by 106 J mol^{-1}. Silicon has a meager effect as 0.3 wt pct addition of Si causes no change in $\Delta G^{\gamma \to \alpha}$ (Figure 1(b)). In this context, a 0.3 wt pct Cr addition changes $|\Delta G^{\gamma \to \alpha}|$ by 36 J mol^{-1} (Figure 1(c)). Mn significantly decreases $\Delta G^{\gamma \to \alpha}$ and a 0.3 wt pct addition of the same element results in a reduction of $|\Delta G^{\gamma \to \alpha}|$ by 70 J mol^{-1} (Figure 1(d)). Carbon, manganese, and chromium additionally have a strong influence on reducing the bainitic transformation temperature.[32–36]

High undercooling (below B_s) triggers bainitic transformation profusely; it not only increases the volume

Table II. Chemical Composition of Investigated Alloys (Weight Percent)

Steel ID	C	Cr	Mn	Si	Mo	B	P	S	N
Alloy I	0.15	3.00	0.54	1.5	0.30	0.004	0.020	0.025	0.02
Alloy II	0.15	0.68	1.60	2.0	0.25	0.004	0.014	0.016	0.02

fraction of bainite but also promotes finer bainitic lath.[37] During austenite decomposition, carbon is rejected into austenite by the nucleating phase and saturates it until the reaction is completed. Thus, a large driving force is required for achieving the fine laths and higher volume fraction of transformation products. Considering the effects of alloying elements, as described previously, two alloys were made in the present investigation. Alloy I was prepared with lower manganese (0.54 wt pct). Lower manganese reduced the hardenability and increased the transformation temperature. So, Cr (3.0 wt pct) was added to compensate the lowering of the transformation temperature and compensate for the loss of hardenability. The steel was further modified with the addition of Mo (0.2 to 0.4 wt pct) to push the pearlite and ferrite bay toward the right. The $\Delta G^{\gamma\to\alpha}$ for alloy I is -615 J mol^{-1} with a B_s temperature of 544 °C. Alloy II was prepared with low Cr (0.68 wt pct) and medium Mn (~ 1.6 wt pct) content for reducing the transformation temperature. Mo (0.20 to 0.4 wt pct) was added to delay the pearlite and ferrite transformation as before. The $\Delta G^{\gamma\to\alpha}$ for alloy II is estimated to be -592 J mol^{-1} at a B_s temperature of 550 °C. In both alloys, Si was added to avoid the formation of carbide within bainite.[27–29] The effectiveness of boron to provide hardenability deals with its ability of segregation at the austenite grain boundary where it prevents the formation of grain boundary allotriomorphic ferrite. However, boron can still form some amount of $Fe_{23}(C, B)_6$ precipitate.[33] This happens at the austenite grain boundary particularly when boron and carbon content become excess. In such cases, the addition of Mo improves the efficiency of B by the intragranular Mo-C cluster. The cluster formation reduces the diffusivity and activity of boron at the austenite grain boundary.

III. EXPERIMENTAL PROCEDURE

A. *Preparation of Heat*

Alloys were prepared in an air induction furnace and $100 \times 100 \times 500$ mm^3 ingots were cast. Ingots were homogenized at 1523 K for 24 hours, followed by forging to ~ 70×70 mm^2 thick bar. The forged bar was air cooled to room temperature. The chemical composition of the alloys is collated in Table II.

B. *Sampling, Its Preparation, and Microscopy*

Standard metallography practices were applied to observe the microstructure under an optical microscope. The samples were polished using emery papers with increasing fineness followed by polishing with 0.6- and 0.1-μm diamond pastes. Subsequently, the samples were etched with 2 pct Nital solution to reveal the microstructure. Samples were examined in the optical microscope (Leica DM300) equipped with an Axio-Vision 4 software system for image analysis. To reveal the finer structural details, the same specimens were studied under a scanning electron microscope (SEM, FEI Nova 430 Nano SEM). Defect characterization and structural characteristics in the sub-nanoscale were investigated in a TEM (TEM, JEOL* JEM 2200FS). For TEM sample preparation, a thin slice from bulk alloy was cut using the electrodischarge machine. The thickness of the slice was reduced to ~ 0.1 mm by mechanical grinding and 3-mm-diameter coupons were produced by shear punching. Further thinning was done by a twin jet electropolisher (Fischione I10) using a mixture of ethanol and Perchloric acid in a ratio of 9:1.

*JEOL is a trademark of Japan Electron Optics Ltd., Tokyo.

C. *Mechanical Testing*

Bulk hardness measurements were done in a Brinel Hardness scale at 3000-kg load with a 10-mm-diameter ball. Five such readings were taken to check the reproducibility of the data. Tensile properties were evaluated per standard ASTM E8-2007 using a cylindrical specimen. Charpy V notch impact testing was performed on samples with dimensions $10 \times 10 \times 55$ mm^3 per standard ASTM E23-2007.Three specimens were tested in each case (for tensile and impact testing) to obtain an average value with standard deviation.

D. *X-ray Diffraction Analysis*

X-ray diffraction was done (Bruker's D8 advance) with a step size of 0.020 in the range of 40 to 100 deg ($= 2\theta$) at 45-kV applied potential and 45-mA current with filtered Cu K_α radiation. Lattice parameters were calculated using Cohen's method, taking care of errors in counter diffractometers.[37–41] The phase fractions were determined using the Maud.[42,43] The carbon concentration in austenite was determined using Dyson and Holmes' equation, which relates the austenite lattice parameter to alloy composition.[44,45]

IV. RESULTS AND DISCUSSION

It has been discussed earlier that fine bainitic lath formation requires lowering of the transformation temperature and enhancement of the driving force.[32–36]

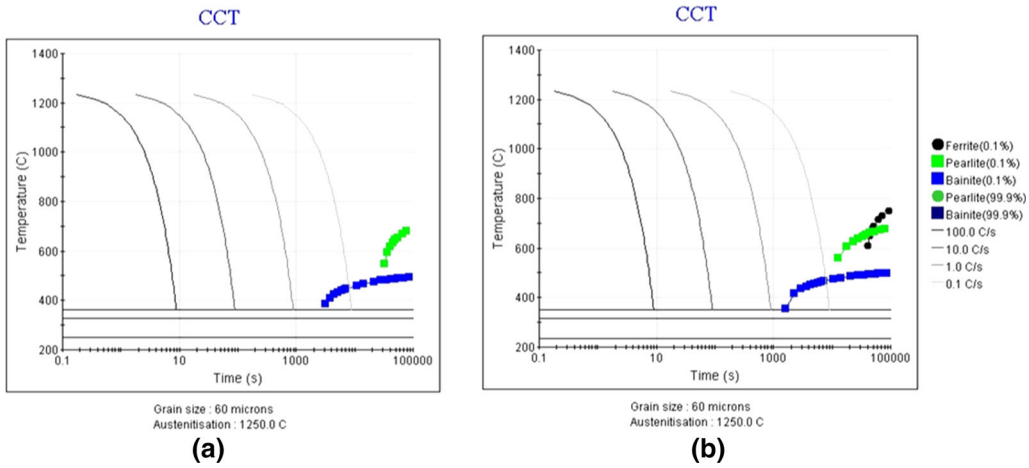

Fig. 2—CCT plots for (*a*) alloy I and (*b*) alloy II.

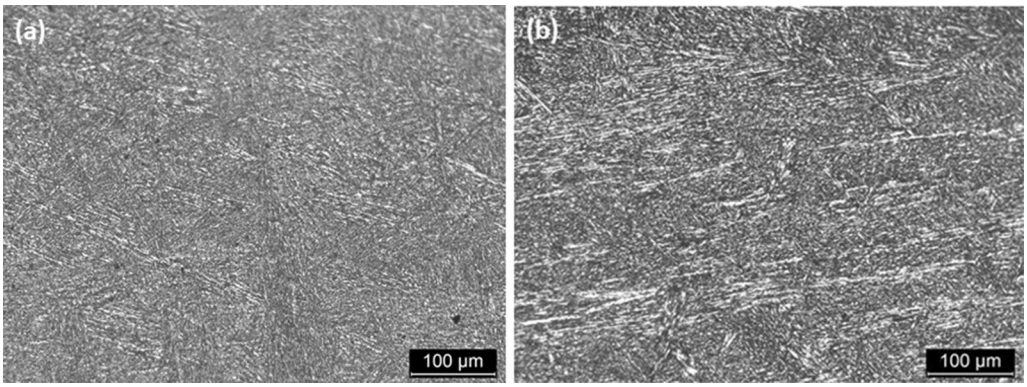

Fig. 3—Optical micrographs of (*a*) alloy I and (*b*) alloy II exhibit uniform distribution of bainite and austenite.

The effect of Cr, Mn, Si, and C on $\Delta G^{\gamma \to \alpha}$ has already been discussed (Figure 1). Carbon plays a significant role in the reduction in the driving force. Thus, carbon was kept at a lower range (~ 0.15). Fine-scale bainitic lath formation requires a low B_s temperature. To keep a balance, Cr was kept at the higher side at ~ 3 wt pct in alloy I, which lowers the bainitic start (B_s) temperature without reducing the driving force for transformation. The combination of the increase in chromium content to 3 wt pct and less manganese content of 0.54 wt pct provides a high driving force for bainitic transformation and a lower bainitic start temperature. Alloy II has higher manganese concentration (~ 1.6 wt pct), which reduced the bainitic start (B_s) temperature. Cr was kept to a lower limit at 0.68 wt pct in this case. Figure 2 shows the CCT plots for the two alloys using JMat Pro software.[46] It is evident from the plots that austenite is getting transformed into bainite during air cooling (0.1 °C/s to 0.5 °C/s) in both specimens.

Figure 3 shows the optical micrographs of alloys I and II exhibiting a uniform distribution of bainite and austenite phase in the microstructure. Feathery bainitic matrix and retained austenite have been revealed in these images (Figures 4 through 6). Fragmented and degenerated acicular bainite in alloy I and elongated acicular bainite with lath morphology in alloy II are depicted in SEM micrographs (Figures 4(a), (b)); these are in good agreement with the reported literature.[47–49] M/A constituents are also observed in both alloys (Figure 4). The white encircled regions in Figure 4 show the presence of blocky M/A constituents formed in alloy I, which are absent in alloy II. Figures 5 and 6 show the bright- and dark-field TEM images depicting the microstructure of bainite and austenite. A selected area diffraction (SAD) pattern confirms the presence of retained austenite and martensite along with bainite (Figures 5 and 6). TEM investigation revealed the absence of carbide precipitation in the matrix. It has been envisaged that the addition of 1.5 to 2.0 wt pct silicon was sufficient to suppress carbide precipitation in the bainite formed during air cooling. The width of the bainitic ferrite plate was measured by the mean lineal intercept $(\overline{L})$

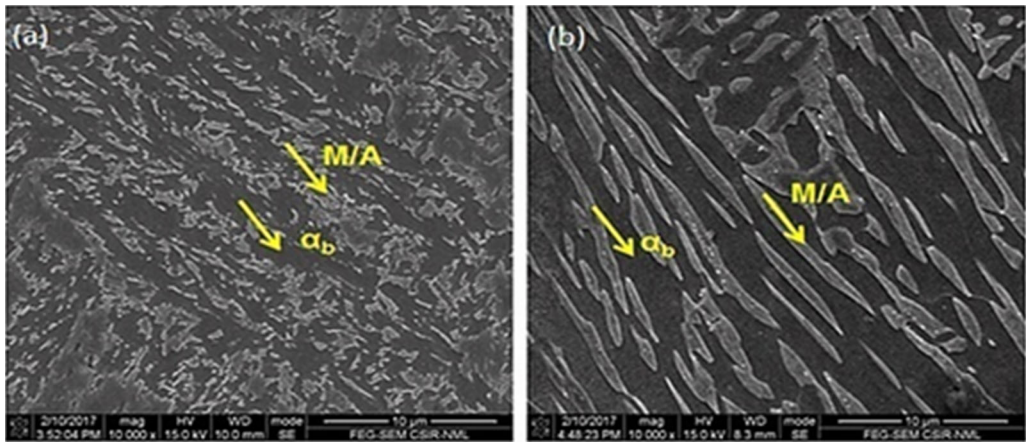

Fig. 4—Scanning electron micrographs of steels: (*a*) alloy I and (*b*) alloy II show bainite (α_b) and M/A constituents.

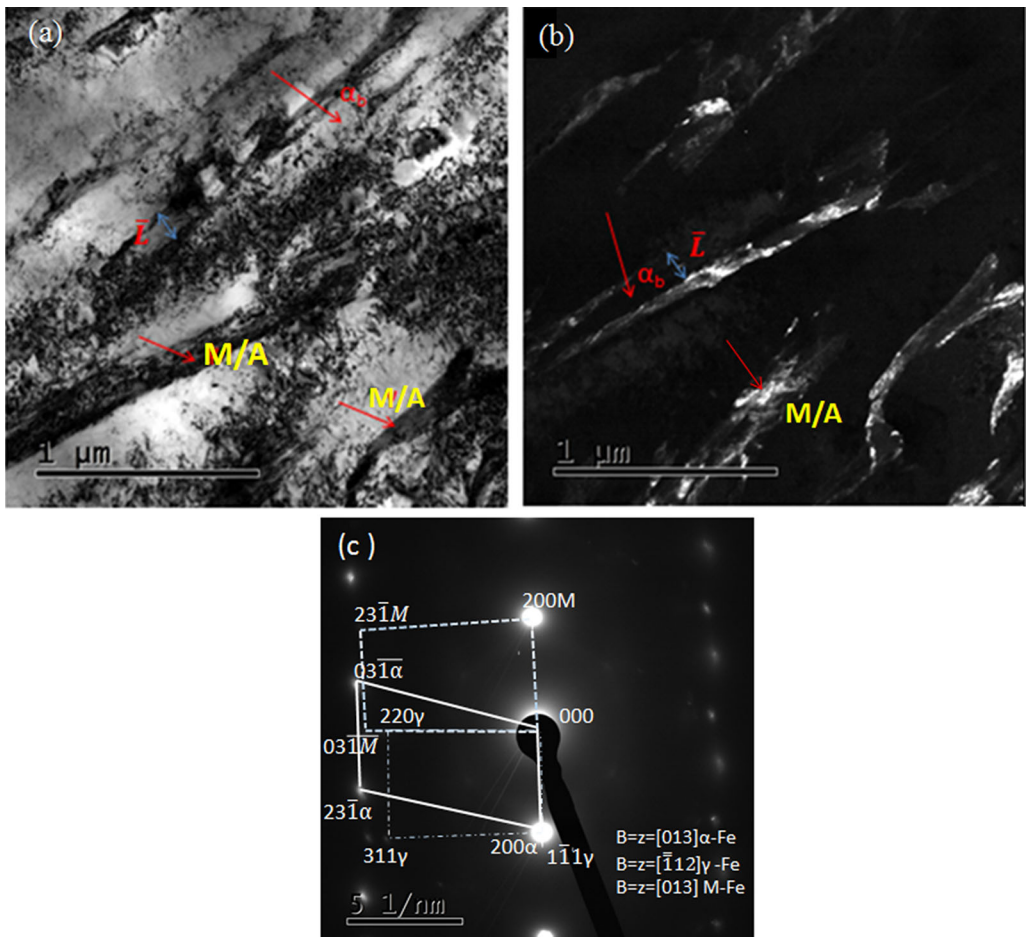

Fig. 5—Transmission electron micrographs of alloy I: (*a*) bright-field imaging; (*b*) corresponding dark-field image; and (*c*) SAD pattern of austenite (γ), martensite (M), and bainite (α_b) phases having $\alpha[013]//M[013]//\gamma[\bar{1}12]$. $\bar{L}$ represents the mean linear intercept of bainite lath.

from TEM images. The true thickness (t) was estimated using equation[23,50]

$$t = \frac{2\bar{L}}{\pi} \qquad [7]$$

The thickness of the bainitic lath was found to be in the order of 100 ± 20 nm for alloy I and 170 ± 20 nm for alloy II. High Cr (~ 3 wt pct) and low Mn (~ 0.6 wt pct) content resulted in a low transformation temperature and a larger driving force for the transformation in alloy

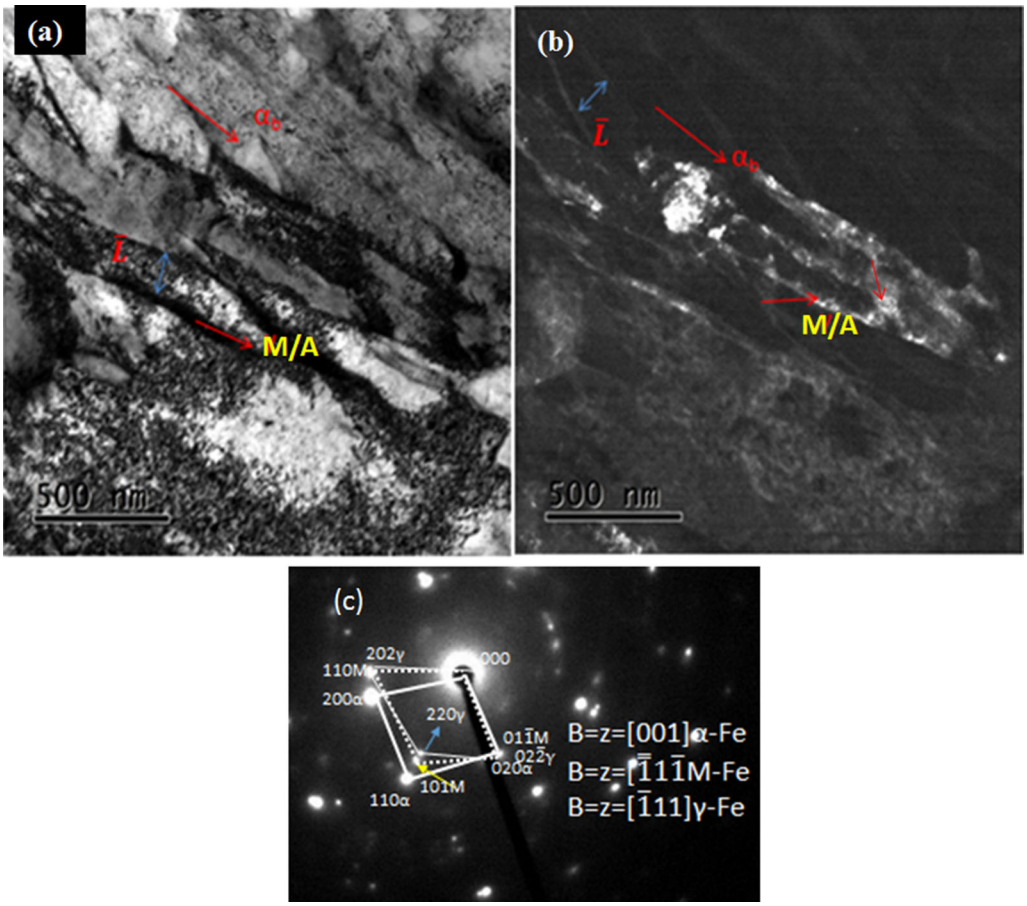

Fig. 6—Transmission electron micrographs of alloy II: (*a*) bright-field imaging; (*b*) corresponding dark-field image; and (*c*) SAD pattern of austenite (γ), martensite (M), and bainite (α_b) phases having $\alpha[001]//\gamma[\bar{1}1\bar{1}]//M[\bar{1}11]$. $\bar{L}$ represents the mean linear intercept of bainite lath.

Table III. Critical Temperatures and Free Energy of Phase Transformation for Investigated Alloys

Steel ID	B_s (K)	M_s (K)	$\Delta G^{\gamma\rightarrow\alpha}$ at B_s (J mol^{-1})
Alloy I	817	680	− 615
Alloy II	823	686	− 592

I than alloy II, as indicated in Table III. The theoretical strength was estimated using Eqs. [1] through [5] for alloys I and II (Figure 7). The strengthening due to solid solution and dislocation was similar in alloys I and II. The strengthening due to bainite lath was higher in alloy I (700 MPa) as compared to alloy II (450 MPa), as shown in Figure 7. This is attributed to the larger driving force for bainite transformation and lower bainitic start temperature for alloy I as compared to alloy II. Thus, the theoretical estimates became at par with the experimental results (Table IV). XRD for alloys I and II exhibited the presence of both γ and α-Fe phases (Figure 8). The volume fractions of different phases are tabulated in Table V.

Alloy I contained a higher volume fraction of retained austenite (~ 17 pct) as compared to alloy II (~ 10 pct). The carbon concentration present in the retained

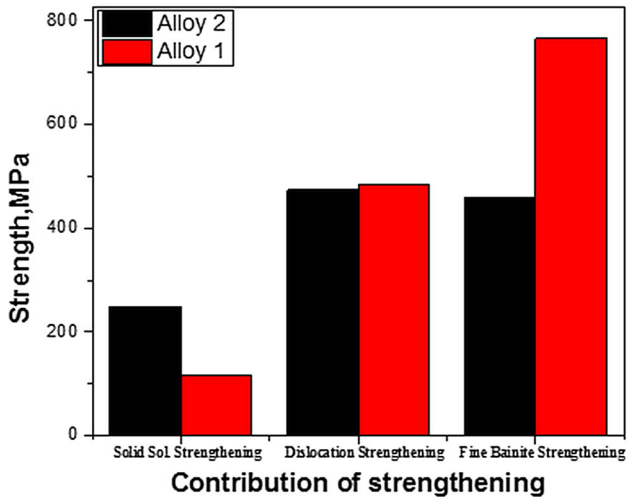

Fig. 7—Calculated theoretical strength of the investigated alloys.

austenite was also estimated through XRD.[38,39] Alloy I with 1.5 wt pct Si has 0.50 wt pct C in retained austenite, whereas alloy II with 2 wt pct Si has 0.66 wt pct C in retained austenite. A higher concentration of Si (2 wt pct) steered greater carbon concentration in retained austenite (0.66 wt pct C) in alloy II as compared

Table IV. Theoretical Prediction and Experimental Validation (at Room Temperature) of Mechanical Properties of Investigated Alloys

Steel ID	Ultimate Tensile Strength (MPa)	Yield Strength (MPa)	Elongation (Pct)	Hardness (BHN)	Toughness (J)
Alloy I	1348 ± 18	835 ± 28	15 ± 1	380 ± 10	20 ± 5
Alloy II	1160 ± 40	801 ± 24	22 ± 2	320 ± 5	40 ± 5

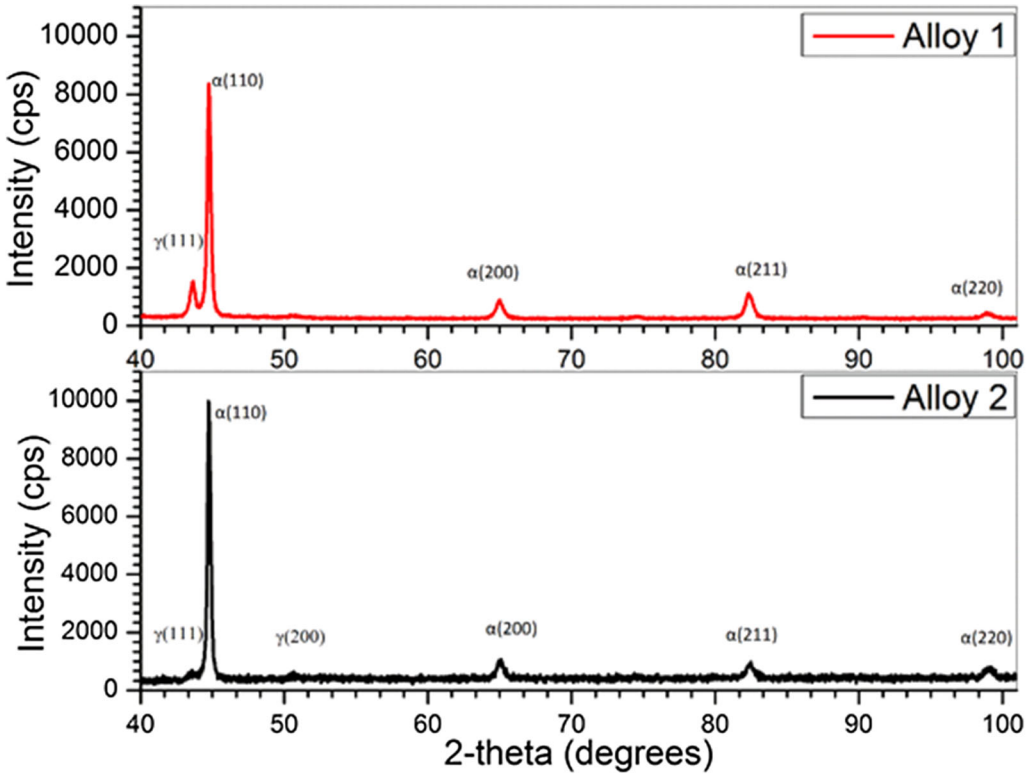

Fig. 8—X-ray characteristic spectra of alloys I and II illustrating the existence of austenite and bainite phases.

Table V. Phase Fraction, Lath Dimensions, Lattice Parameter, and Carbon (Weight Percent) in Retained Austenite as Calculated from X-ray Diffraction Study of Steels

Steel ID	V_α (Pct)	V_M (Pct)	V_γ (Pct)	Lath Thickness (nm)	a_α (Å)	a_γ (Å)	x_α (Wt Pct)	x_γ (Wt Pct)
Alloy I	74	9	17	100 ± 20	2.869	3.59	0.033	0.50
Alloy II	80	10	10	170 ± 20	2.869	3.60	0.033	0.66

to alloy I (0.50 wt pct C).[51] On the other hand, alloy I exhibited poor toughness. Strength and toughness of any alloy do not depend on the existing microstructure only, but also on the strain-induced phase transformation that may occur during mechanical tests. Alloy II exhibited a carbon concentration of ~ 0.66 wt pct within 10 vol pct of retained austenite. On the contrary, alloy I had ~ 0.5 wt pct C in 17 vol pct retained austenite. The partitioning of carbon in the surrounding retained austenite shifted the M_s temperature for alloy I to 519 K (246 °C) and for alloy II to 399 K (126 °C). The M_d temperature for 50 pct martensite formation for the two alloys was calculated by an empirical formula, as reported by Angel *et al.*,[52] and the 30 pct deformation $M_d(50/30)$ temperature for alloys I and II was found as 388 K (115.3 °C) and 335.8 K (62.8 °C), respectively. The deformed samples after tensile testing of alloys I and II were examined in a TEM. In the case of alloy I, metastable retained austenite transformed into martensite with lath thickness ~ 4 nm (Figure 9). Under the

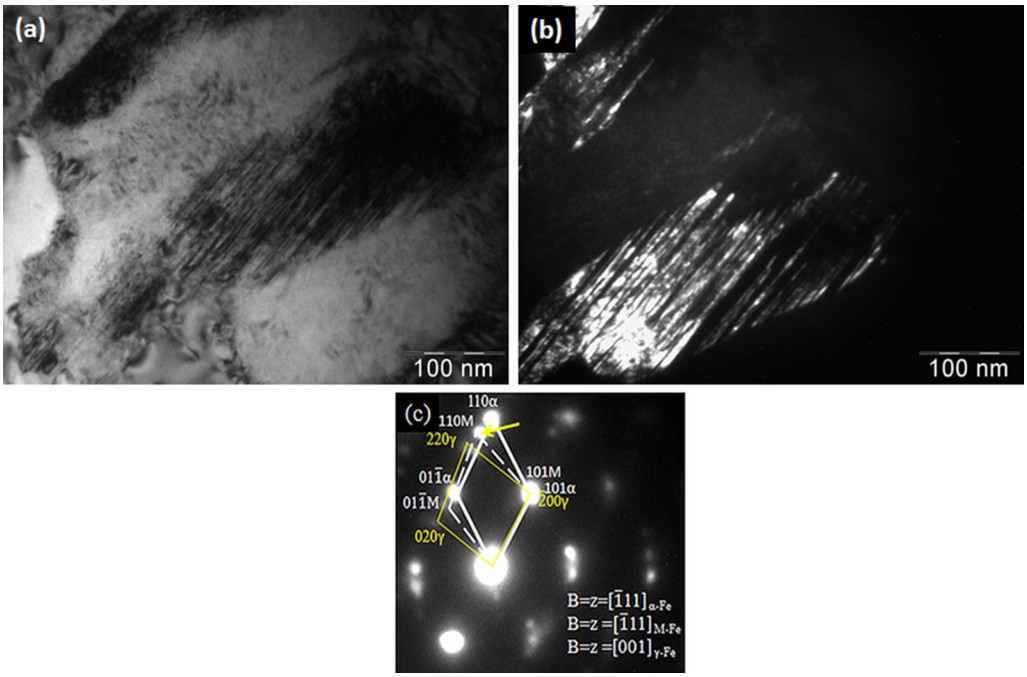

Fig. 9—Transmission electron micrographs of mechanically deformed samples of alloy I: (*a*) bright-field imaging showing formation of martensite from the retained austenite; (*b*) corresponding dark-field image; and (*c*) SAD pattern exhibiting the presence of martensite, ferrite, and retained austenite.

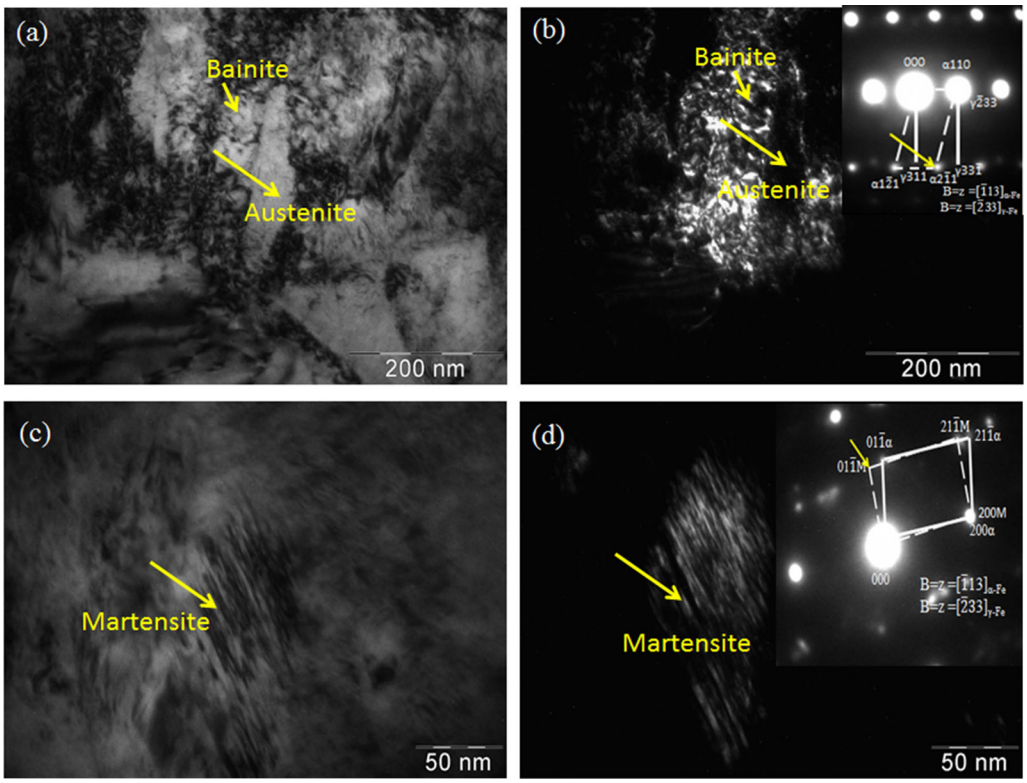

Fig. 10—Transmission electron micrographs of mechanically deformed samples of alloy II: (*a*) bright-field imaging showing few stable austenite remained untransformed, (*b*) corresponding dark-field image, (*c*) bright-field imaging showing few retained austenite transformed to martensite, (*d*) corresponding dark-field image.

same state of deformation, alloy II also exhibited retained austenite to martensite transformation with an average lath thickness of ~ 2 nm (Figure 10). The reason for the difference in the lath width of martensite between the two alloys was twofold: alloy II contained a smaller quantity of retained austenite with a lower value of M_d temperature in comparison to alloy I.[31] Thus, most of the austenite remained unchanged for alloy II (Figure 10). Untransformed austenite (~ 90 ± 10 nm thick) contained a high dislocation density (Figure 10). The stability of retained austenite in alloy II and the formation of fine martensite facilitated improvement in toughness and elongation (~ 22 ± 1 pct) as compared to alloy I. Alloy I exhibited relatively coarser M/A constituents (Figure 4(a)), which further deteriorated the toughness of the steel. The higher hardness and tensile strength of alloy I with respect to alloy II might be attributed to a greater extent of austenite to martensite transformation in the case of the former compared to the latter during uniaxial deformation.

Thus, the novel composition with 0.15 wt pct C and 3 wt pct Cr was developed with an extraordinary strength of 1348 ± 18 MPa and elongation of 15 ± 1 pct, which can be used efficaciously in various applications. From the open literature, it is evident that continuously cooled bainitic steel might be able to achieve a tensile strength of 1213 to 1370 MPa and elongation of 15 to 21 pct for a carbon content of 0.25 to 0.35 wt pct.[4,5,8] Ni was also used in the range of 3.5 wt pct, which made the alloy costly.[4] Thus, a logical modification in alloy design along with the appropriate thermal treatment in the present investigation delivers a promising new generation of ultrafine carbide-free bainitic steel of improved strength and hardness (380 ± 10 BHN).

V. SUMMARY

In the present investigation, two types of alloys were prepared with a variation in Mn, Cr, and Si concentration. Alloy design was done theoretically based on the kinetics and thermodynamics of phase transformation along with the prediction of mechanical properties. Experimentally, the microstructure and mechanical properties were evaluated. The major findings are as follows.

1. Alloys were designed in such a way that carbide-free bainite was obtained by air cooling. Alloy I exhibited higher driving force for bainitic transformation than alloy II. This high driving force resulted in finer lath width in alloy I as compared to alloy II.
2. During phase transformation, carbon was partitioned and migrated to retained austenite. Retained austenite of alloy I contained less carbon than the retained austenite of alloy II. This reduced the stability of austenite for alloy I.
3. Fine-scale bainitic lath provided superior strength and hardness for alloy I in comparison to alloy II.
4. Metastable retained austenite transformed to martensite during tensile and impact tests. Martensite formation was dominant for alloy I due to the lesser stability of retained austenite with respect to alloy II. The high volume fraction of hard constituent (martensite) reduced the ductility and toughness of alloy I.
5. Improved toughness and ductility of alloy II were due to the presence of fine-scale martensite (~ 2 nm) with untransformed austenite having adequate dislocation density.
6. Bainitic steel with ~ 0.15 wt pct C was produced in lab scale by the normal air cooling route. Alloy I with a strength of 1348 ± 18 MPa, hardness of 380 ± 10 BHN, and elongation of 15 ± 1 pct shows a good combination of mechanical properties.

ACKNOWLEDGMENTS

The authors are thankful to the director, CSIR–National Metallurgical Laboratory, for his kind permission to publish this work. The fruitful technical discussion with Dr. M. Ghosh, Sr. Scientist, CSIR-NML, is gratefully acknowledged.

REFERENCES

1. H.K.D.H. Bhadeshia and D.V. Edmonds: *Met. Sci.*, 1980, vol. 14, pp. 41–49.
2. R.C.D. Richardson: *Wear*, 1967, vol. 10, pp. 291–309.
3. G. Gomez, T. Perez, and H.K.D.H. Bhadeshia: *Mater. Sci. Technol.*, 2009, vol. 25, pp. 1501–07.
4. G. Gomez, T. Perez, and H.K.D.H. Bhadeshia: *Mater. Sci. Technol.*, 2009, vol. 25, pp. 1508–12.
5. T. Sourmail, V. Smanio, F.G. Caballero, J. Cornide, C. Capdevilla, C. Garcia-Mateo, T. Chandra, M. Ionescu, and D. Mantovani: *Mater. Sci. Forum*, 2012, vol. 706, pp. 2308–13.
6. C. Garcia-Mateo, F.G. Caballero, and H.K.D.H. Bhadeshia: *ISIJ Int.*, 2003, vol. 43, pp. 1238–43.
7. C. Garcia-Mateo and F.G. Caballero: *ISIJ Int.*, 2007, vol. 45, pp. 1736–40.
8. S. Das and A. Haldar: *Metall. Mater. Trans. A*, 2014, vol. 45A, pp. 1844–53.
9. K. Wang, Z. Tan, G. Gao, B. Gao, X. Gui, R.D.K. Misra, and B. Bai: *Mater. Sci. Eng. A*, 2016, vol. 675, pp. 120–27.
10. D. Seferian: *Metallurgy of Welding,* Mashgiz, Moscow, 1963, p. 268 (**in Russian**).
11. P. Clayton and N. Jin: *Wear*, 1996, vol. 200, pp. 74–82.
12. P. Clayton and R. Devanathan: *Wear*, 1992, vol. 156, pp. 121–31.
13. J. Kalousek, D.M. Fegrdo, and E.E. Laufer: *Wear*, 1985, vol. 105, pp. 199–222.
14. P.H. Shipway, S.J. Wood, and A.H. Dent: *Wear*, 1997, vols. 203–204, pp. 196–205.
15. E. Vuorinen, A. Linström, P. Rubin, E. Navara, and M. Oden: *Pellets 2006: Proc. 2nd World Conf. on 'Pellets,'* Jonkoping, Sweden, June 2006, Swedish Bioenergy Association (SVEBIO), Stockholm, 2006, pp. 151–55.
16. H.-S. Fang, Q. Li, B.-Z. Bai, Z.-G. Yang, Dong.-Yu. Liu, and F.-B. Yang: *Int. J. ISSI*, 2005, vol. 2, pp. 9–18.
17. X. Kong and C. Qiu: *J. Mater. Sci. Technol.*, 2013, vol. 29, pp. 446–50.
18. L. Zhang, A. Pittner, T. Michael, M. Rhode, and T. Kannengiesser: *Sci. Technol. Weld. Join.*, 2015, vol. 20, p. 371.
19. E. Keehan, L. Karlsson, H.-O. Andrén, and H.K.D.H. Bhadeshia: *Sci. Technol. Weld. Join.*, 2006, vol. 11, pp. 9–18.
20. H.K.D.H. Bhadeshia: *Bainite in Steels: Theory and Practice*, 3rd ed., Maney Publishing, Leeds, 2015, p. 286.
21. F.B. Pickering and T. Gladman: *Iron Steel Inst.*, 1963, vol. 81, p. 10.

22. A.S. Keh and S. Weissmann: *Electron Microscopy and the Strength of Crystals*, Interscience, New York, NY, 1963, pp. 231–300.
23. C. Garcia-Mateo: *Mater. Charact.*, 2016, vol. 122, pp. 83–89.
24. A.A.B. Sugden and H.K.D.H. Bhadeshia: *Metall. Trans. A*, 1988, vol. 19A, pp. 1597–1602.
25. J. Daigne, M. Guttmann, and J.P. Naylor: *Mater. Sci. Eng.*, 1982, vol. 56, pp. 1–10.
26. S.B. Singh and H.K.D.H. Bhadeshia: *Mater. Sci. Eng. A*, 1998, vol. 245, pp. 72–79.
27. H.K.D.H. Bhadeshia and D.V. Edmonds: *Mater. Sci.*, 1983, vol. 17, pp. 420–25.
28. A.R. Kiani-Rashid: *J. Alloys Compd.*, 2009, vol. 474, pp. 490–98.
29. H.K.D.H. Bhadeshia: *Bainite in Steels*, The Institute of Materials, Cambridge University Press, Cambridge, UK, 1992.
30. E. Kozeschnik and H.K.D.H. Bhadeshia: *Mater. Sci. Technol.*, 2013, vol. 4, pp. 343–47.
31. Mathew Peet and H.K.D.H. Bhadeshia: *MUCG 83. Mater. Algor. Proj.*, 2011.
32. K.W. Andrews: *J. Iron Steel Inst.*, 1965, vol. 203, pp. 721–27.
33. W. Steven and A.G. Haynes: *J. Iron Steel Inst.*, 1956, vol. 183, pp. 349–59.
34. T. Kunitake and Y. Okada: *J. Iron Steel Inst.*, 1998, vol. 84, pp. 137–41.
35. J.S. Kirkaldy and D. Venugopalan: in *Phase Transformations in Ferrous Alloys,* A.R. Marder and J.I. Goldstein, eds., TMS-AIME, Warrendale, PA, 1984, p. 125–48.
36. Y.-K. Lee: *J. Mater. Sci. Lett.*, 2002, vol. 21, pp. 1253–55.
37. H.K.D.H. Bhadeshia and D.V. Edmonds: *Acta Metall.*, 1980, vol. 28, pp. 1265–73.
38. S. Khare, K. Lee, and H.K.D.H. Bhadeshia: *Int. J. Mater. Res.*, 2009, vol. 100, pp. 1513–20.
39. K. Yamanaka and Y. Ohmori: *ISIJ*, 1977, vol. 17, p. 92.
40. M.U. Cohen: *Rev. Sci. Instrum.*, 1935, vol. 6, pp. 68–74.
41. B.D. Cullity: *Elements of X-ray Diffraction*, 2nd ed., Addison-Wesley Publishing Company Inc., Palo Alto, CA, 1978, pp. 363–66.
42. L. Lutterotti, S. Matthies, D. Chateigner, and S. Ferrari: *Mater. Sci. Forum*, 2002, vols. 408–412, pp. 1603–08.
43. G. Ischia, H.-R. Wenk, L. Lutterotti, and F. Berberich: *J. Appl. Cryst.*, 2005, vol. 38 (2), pp. 377–80.
44. D.J. Dyson and B. Holmes: *J. Iron Steel Inst.*, 1970, vol. 208, pp. 469–74.
45. M.J. Peet: http://mathewpeet.org/thesis/programs/, 2009.
46. JMat Pro: http://www.sentesoftware.co.uk/jmatpro.aspx.
47. L.J. Habraken and M. Ecomopoulos: *Transformation and Hardenibility in Steels*, Climax Molybdenum Co., Ann Arbor, MI, 1967, pp. 69–106.
48. B.L. Bramfitt and J.G. Speer: *Mater. Trans. A*, 1990, vol. 21A, pp. 817–29.
49. F.G. Caballero, H. Roelofs, S. Hasler, C. Capdevila, J. Chao, J. Cornide, and C. Garcia-Mateo: *Mater. Sci. Technol.*, 2012, vol. 28, pp. 95–102.
50. L.C. Chang and H.K.D.H. Bhadeshia: *Mater. Sci. Technol.*, 1995, vol. 11, pp. 874–81.
51. H. Huang, M.Y. Sherif, and P.E.J. Rivera-Diaz-del-Castillo: *Acta Mater.*, 2013, vol. 61, pp. 1639–47.
52. T. Angel: *J. Iron Steel Inst.*, 1954, vol. 177, pp. 165–74.